Scrap metal classification using magnetic induction spectroscopy and machine vision

DOI:
10.1109/TIM.2023.3284930

Document Version
Accepted author manuscript

Scrap metal classification using magnetic induction spectroscopy and machine vision

Kane C. Williams, *Student Member, IEEE*, Michael D. O'Toole, *Member, IEEE*, Anthony J. Peyton

***Abstract*—The need to recover and recycle material towards building a circular economy is increasingly a global imperative. Non-ferrous metals in particular are highly recyclable and can be extracted using processes such as eddy current separation. However, their further separation into recyclable groups based on metal or alloy continues to pose a challenge. Recently, we proposed a new technique to discriminate between non-ferrous metals: Magnetic induction spectroscopy (MIS) measures how a metal fragment scatters an excitation magnetic field over different frequencies. MIS is related to conductivity, which can be used to classify the fragment according to this property.**

In this paper, we demonstrate for the first time the use of MIS with machine learning to classify non-ferrous scrap metals drawn from commercial waste streams. Two approaches are explored: (1) MIS over a bandwidth from 3 kHz to 90 kHz, and (2) the combination of MIS with physical colour of the metal samples. We show that MIS alone can obtain purity and recovery rates >80% for most metal groups and waste streams, rising to >93% for stainless steel. The exception was the Zorba waste stream where the mix of aluminium alloys within the sample set led to poor conductivity contrasts. The introduction of colour substantially improved results in this case, increasing purity and recovery rates by 20-35 percentage points. Of the machine learning models tested, we found that random forest, extra trees and support vector machine algorithms consistently achieved the highest performance.

***Index Terms*—Classification algorithms, Electromagnetic induction, Machine vision, Recycling, Waste recovery**

I. Introduction

An accurate and economic separation technique is essential to allow non-ferrous metals to be recovered, recycled, and reused. The advantages of returning non-ferrous metal to the supply chain are substantial. For instance, materials such as aluminium and copper are highly recyclable; aluminium produced from mined Bauxite ore requires 186,262 MJ of energy to acquire 1000 Kg of primary aluminium, whereas secondary (recycled) aluminium requires only 11,690 MJ [1]. This substantial energy saving means reduced CO2 emissions and impact on the climate. There is international pressure to improve the rate of metal recycling, recognising the need to move to a more sustainable 'Circular economy' [2]. In Europe, for example, EU directives (2000/53/EC) and (2012/19/EU) address the need for materials recovery in end-of-life vehicles and waste electrical and electronic equipment (WEEE); both prominent sources of non-ferrous metal.

Non-ferrous metals are primarily separated from source waste streams by eddy current separation. This process uses a high-speed rotating drum embedded with permanent magnets to induce eddy-currents in the fragment, which in turn, develop Lorentz forces. In highly conductive fragments, i.e. non-ferrous metals, the Lorentz force is sufficient to eject the sample from the conveyor, whereas poorly conducting fragments are allowed to free-fall from the conveyor. This means the eddy-current separator (ECS) is limited by the geometry of the waste fragments. It can be difficult to generate large repulsive forces with smaller-sized metal pieces, or long-thin elements such as wires where it is more difficult for eddy-currents to circulate [3]. High density and low-conductivity material is also difficult to eject. The resultant product of the ECS is a mix of non-ferrous metals which must be further separated to be recyclable and yield full value.

Many challenges remain in sorting this non-ferrous metal mix reliably, efficiently and at scale. These metals need to be sorted into their base elements (aluminium, copper, zinc, etc), and in some cases, further sorted by alloy family. Tramp elements within an alloy make them difficult to recycle. Small amounts within the recyclate are allowed at a specific rate, but high rates can make the produced metal brittle [4]. Tramp elements become more of an issue in aluminium, where they are difficult to remove [3]; this makes it essential to recycle some aluminium sources into clean alloy families, increasing the complexity of recycling processes and the risk of cross-contamination that undermines alloy sustainability.

There are several methods for sorting non-ferrous metals, each with advantages and disadvantages as summarised in Table I. A common approach is sorting by hand, using the worker's judgement to sort by colour and physical characteristics [3]. Manual sorting is only economical in regions where labour costs are low. Regions such as Europe and the United States have tended to export their waste, the volume of which has seen substantial growth over the last 20 years [3]. It is claimed that manual sorting can achieve classification accuracies up to 99% [5]. The sustainability of manual sorting in other countries has been challenged, not least on environmental costs of waste transport. Sink-float systems offer a less labour intensive, conceptually simple solution that uses the different densities of metals for separation. Slurries of water, sand and air are used to create different gravitational drums that separate the metal [3]. The sink-float method struggles

 This work was supported by the UK Engineering and Physical Sciences Research Council (P122584) and the Innovate UK (contract ref 72207)

The authors are with the Department of Electrical and Electronic Engineer- ing, The University of Manchester, Manchester M13 9PL, U.K. (e-mail: kane.williams@manchester.ac.uk; michael.otoole@manchester.ac.uk; a.peyton@manchester.ac.uk).

to separate hollow and boat-shaped materials. There is a high cost of maintaining a constant gravitational density [3], and the process creates environmental waste, such as contaminated water, which requires treatment.

The gold standard methods to classify non-ferrous scrap metal are Laser-Induced Breakdown Spectroscopy (LIBS) and X-ray methods, such as X-ray transmission (XRT) and X-ray fluorescence (XRF). LIBS and XRF are commonly used to establish ground-truth metal composition using handheld analysers or laboratory instruments [6], [7], hence their discrimination capability is high. In operation, they work downstream of ECS, separating the mixed non-ferrous metal product that results. As dry sensor-based methods, these techniques can only passively interrogate the sample as they pass across the conveyor and must be paired to ejector mechanisms, typically air-jets, to provide the physical separation of the metal pieces.

LIBS is a technique that classifies metals by laser ablating the surface of the metal to generate a plasma to analyse composition [8]. Fast conveyor speeds, however, can makes it difficult to target the laser where precise multiple firings are required to obliterate surface contaminants before measuring the plasma [9], [10]. It has been proposed to use an additional camera system to identify flat and uncontaminated points on the sample [8], however, this builds complexity and implementing a near-3D camera under high-speed operation is still a significant technical challenge. XRT uses a high intensity X-ray beam to measure absorption across the metal piece [10]. This allows XRT to separate light metal (aluminium) from heavy metals (copper and brass). This technique is not affected by surface contaminants, however it is unable to sort metals of similar density [11], [12]. XRF emits low energy radiation on to the surface of a metal, causing excited low-energy electrons to eject [13]. The space left is filled by high energy electrons, which release an elemental specific fluorescence [13]. Like LIBS, XRF is susceptible to surface contamination and can be difficult to use for elements with very low characteristic radiation, such as aluminium, silicon and magnesium [3]. Spectral ratios for aluminium alloys, for example, tend to be determined by their major alloying elements [3].

LIBS and X-ray techniques, while offering good performance and capability, are generally very expensive and face limitations when translated to high-throughput metals classification, where typical commercial conveyor speeds can operate between 2 to 3 m/s. There is still much interest within the state-of-the-art for low-cost, and industrially practical solutions, either as alternatives to LIBS and X-ray or to complement them by providing a pre-sorting stage. For instance, the 'Electrodynamic sorting technology' developed recently at the University of Utah [14], [15], uses a tuneable or variable frequency ECS system to be able to sort different metals and smaller fragment. The authors highlight some success extracting aluminium from Zorba [16], brass, copper and other aluminium alloys [14], although in the latter results were drawn from spherical test samples rather than genuine scrap.

Optical methods, like manual sorting, uses colour characteristics to sort metals, although across more wavelengths compared to the human eye. Li et al. [17] explored deep learning and superpixel optimization with an RGB image, where their proposed algorithm achieved an average precision of 98%, which used 15 samples of aluminium and copper pieces. Hyperspectral imaging (HSI) measures a wider spectrum beyond the RGB wavelengths provided by a standard camera, returning a rich feature set for classification. HSI methods have achieved classification accuracies of 96.87% [18] and 98.36% [19] with WEEE scrap metal and 80 to 97% for brass, iron, copper, aluminium, and nickel classification [20]. Although HSI provides good classification, the high dimensional vector associated with each pixel combined across the whole image creates a heavy computational load [18]; this limits the speed of the conveyor to allow time for processing. HSI classification has been reported on conveyor speeds running at up to 2.28 m/s; an improvement on previous methods of $<$1 m/s [18].

This study explores the use of magnetic induction or electromagnetic sensors for non-ferrous metal classification. These sensors are generally lower cost than other methods and are well-suited to fast-moving conveyors and the constraints of high-throughput operation. They operate on similar principles to eddy-current separators, in that an oscillating magnetic field is used to induce eddy-currents in the sample. However, these eddy-currents are too small to induce appreciable Lorentz forces, rather it is the resultant secondary magnetic field generated by these eddy-currents that is used to interrogate the characteristics of the metal (i.e. the mutual inductance). This decoupling of ejection method from the magnetic response means that we can potentially classify to finer conductivity contrasts between metals and larger fragment shape variability than ECS, reliant as it is on developing sufficient ejection forces and predictable piece trajectories. Common to the LIBS, X-ray and the optical methods, the magnetic induction sensors must be paired with a physical ejection mechanism to separate the pieces when classified. In contrast, magnetic induction is not influenced by surface contaminants as eddy currents can penetrate the conductive surface of the metal piece.

Magnetic induction sensors have shown some efficacy in separating the different metals of the non-ferrous metal mix produced by eddy-current separation. Messina et al. [21] explored the use of narrowband low-frequency excitations (700 Hz to 5 kHz) and pulsed magnetic fields [12]. This system showed good results for separating metals with high conductivity contrasts, such as low conductivity stainless steel, from other non-ferrous with high conductivity, including bronze, brass, zinc, magnesium, aluminium and copper. Recovery and purity rates between 90 and 100% were reported for stainless steel, whereas recovery and purity were generally below 80% for the other metals. Kutila et al. [22] extended this approach by combining a magnetic sensor with optical system, which could be operated combined or separately. The results showed a similar range of 80% to 95% purity and recovery rates for stainless steels and the separation of reddish metals (copper and brass). Performance was found to be impacted by industrial conditions, including machine vibration, ambient light, and reflections.

We propose to use magnetic induction spectroscopy (MIS) for metals classification. This approach, in contrast to the magnetic induction methods described, uses broadband excitations to obtain mutual inductance measurements across several

frequencies from 3-90 KHz. This broadband spectrum captures the interesting region where skin-depth takes effect, returning measurements which are to differing degrees a function of conductivity and sample geometry (lower frequencies) or sample geometry only (higher frequencies). MIS has been used extensively in non-destructive evaluation research, including surface crack detection [23], lift-off distance and characterisation of metals [24], and estimating thickness of metallic films [25]. MIS has also been used for classification research into metal detection and landmine identification [26] and landmine detection combined with ground penetrating radar [27]. For non-ferrous scrap metal classification, O'Toole et al. developed a dual-frequency MIS system using mixed pairs of excitation frequencies from 3 kHz to 64 kHz [28]. This system was able to classify manufactured scrap pieces in brass, copper, and aluminium with average purity and recovery rates of 92%. However, performance fell to recovery rates of 80% and purity rates of 55% to 80% when tested on scrap metal drawn from commercial waste, where sample morphology and lift-offs from sensing coils were more variable [9]. MIS has also been reported for classification of batteries within waste streams, where notable differences in the spectra were observed across D, AA, AAA and 9V/Eblock cells [29].

In this paper, we examine for the first time the use of broadband multi-frequency magnetic induction spectroscopy to classify non-ferrous scrap metals. As described, magnetic sensors and MIS systems pose a potentially low-cost, industrially robust, general solution to sorting non-ferrous metal mixes output from eddy-current separators, compared to techniques such as LIBS and X-rays. This method can in principle sort any metal, grade, or alloy provided that conductivity contrasts are sufficient, and unlike most other sensor-based approaches, is unaffected by surface contaminants. We advance on previous work by using multiple frequency components across a broadband spectrum from 3-90 kHz and combining these frequency components as features in a machine learning algorithm. In contrast, our previous work only considered two components [28]. By sweeping across the full frequency range, we obtain the full shape characteristics of the spectra as eddy-current penetration diminishes according to the skin-depth effect.

The specific contributions of this paper are threefold: We first demonstrate the capability of using multi-frequency MIS measurements for metals classification by using a static swept frequency test rig, combined with machine learning algorithms to interpret the spectral response and deliver a metal classification. Secondly, we establish the efficacy of different machine learning models for MIS classification, using an expansive sample set of 445 genuine non-ferrous scrap metal pieces drawn from six distinct pre-sorted commercial waste streams. We report the optimal results that can be achieved. Thirdly, we show the impact of combining MIS with some simple metal colour parameters as additional features to support classification. This is based on our findings that some metals with poor conductivity contrasts, such as brass and cast aluminium, conveniently have high colour contrasts. This invites the exciting possibility of using multi-sensor systems, enhancing and mitigating the strengths and weaknesses of individual sensors by their combination.

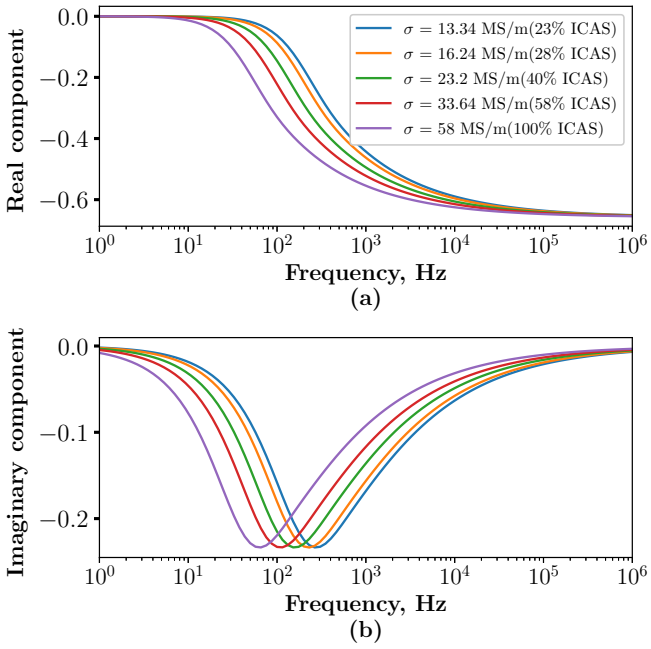

Fig. 1. The real (a) and imaginary (b) components of different conductive spheres of radius 20 mm, measured at a point 3 mm from the surface.

II. Theory

A. Magnetic induction spectroscopy

To understand how magnetic induction spectroscopy can be used to determine the conductivity of different metals, the analytical formulation of a conductive sphere in free space can be used [30]. Define a as the radius of the sphere, σ as its conductivity and its permeability $\mu = \mu_0 = 4\pi \times 10^{-7}$. The conductive sphere is centred at the origin and is within a uniform magnetic field acting along an axis Z, oscillating at frequency f. This field induces eddy currents within the object that flow in the azimuthal direction [31]; these eddy currents induce a secondary magnetic field. If we take a point z along the Z-axis outside the sphere ($z > a$), we can calculate H_{rx} and H_{ex}, which are the complex components of the secondary magnetic field and excitation respectively, using the following,

$$\frac{H_{rx}}{H_{ex}} = -\frac{3a^3}{z^3}\left(\frac{1}{\alpha^2} + \frac{1}{3} - \frac{\cosh\alpha}{\alpha\sinh\alpha}\right) \tag{1}$$

$$\alpha = (i2\pi f\sigma\mu)^{\frac{1}{2}}a$$

Fig. 1 shows the real and imaginary component of H_s/H_{ex} at a point z, 3 mm from the surface of a sphere with a radius of 20 mm. The conductivity of the sphere is varied across a range similar to the metal samples discussed in this paper. It can be seen from Fig. 1 that the peak of the imaginary component shifts lower in frequency when conductivity increases. Fig. 1 also shows that regardless of conductivity, all the curves reach the same asymptote and the only visible difference is between the frequency of convergence. As the frequency increases, the eddy currents flow closer to the surface of the object; this is the skin depth effect [32]. The negligible skin depth at high frequency causes the asymptote of the real component to not change with conductivity [28]. Fig. 2 shows the real and imaginary component of H_{rx}/H_{ex} at z, which is again 3 mm

TABLE I
SUMMARY OF THE ADVANTAGES AND DISADVANTAGES OF SORTING TECHNIQUES FOR NON-FERROUS SCRAP METALS.

Sorting techniques	Separation parameter	Advantage (+) and disadvantage (-)
Eddy current separator (ECS)	Conductivity	+ Does not require additional equipment to eject pieces. - Cannot eject small metal pieces and wire. - Requires the user to manually set the separation bin line. - Generally, only suitable for extracting non-ferrous metals from non-metals.
Manual sorting	Colour and density	+ Low cost. - Accuracy and speed depend on operator experience. - Economical only with low-wages.
Sink and Float	Density	+ Can separate large quantities of metal into light and heavy metal. - High initial outlay, requiring processing plant. - Produces environmental waste that needs to be treated.
XRT	Density	+ Not affected by surface contaminants. - Requires additional radiation safety measures.
XRF	Elemental composition	+ Wide range of metals/alloys can by classified. - Metals with low radioactive characteristics are difficult to classify. - Requires additional radiation safety measures. - Susceptible to surface contamination. - High cost
LIBS	Elemental composition	+ Wide range of metals/alloys can by classified. - Susceptible to surface contamination. - High cost
Optical cameras	Colour	+ Faster classification than manual sorting. - Susceptible to surface contamination present.
HSI	Colour (Expanded wavelengths)	+ Wider set of wavelengths available for classification compared to optical camera. - Takes longer to compute than an optical camera. - Susceptible to surface contamination present.
Electrodynamic sorting	Conductivity	Similar to ECS + Able to sort between non-ferrous groups, e.g. aluminium from Zorba.
Magnetic induction	Conductivity	+ Immune to surface contaminants. + Does not require a line of sight. - Metal pieces should be close to the sensor, which could be problematic if the conveyor or pieces bounce.
Magnetic induction spectroscopy*	Conductivity	Same as magnetic induction + Multiple frequencies for more diverse classification feature set + Potentially improved performance with respect to the conductivity contrasts and shape variability.

*Technique explored in this paper individually and in combination with optical cameras.

away from the surface of the sphere with a fixed conductivity of 16.24 MS/s (28% ICAS). The radius of the sphere ranges between 3 and 90 mm. It can be seen from Fig. 2 that the size of the sphere affects the frequency and height of the imaginary peak and the height of the asymptote of the real component.

B. Classifiers

In the following section, we describe the different classification methods used. These methods are chosen as they work well with a small number of inputs, and the structure of the algorithms is easy to explain and visualise.

Support vector machines (SVM) are a commonly used machine learning algorithm that use hyperplanes to partition the feature-space. Support vector machines can perform linear and nonlinear classification. Nonlinear classification is achieved by a polynomial or radial basis function (RBF). The nonlinear SVM polynomial and RBF perform their own unique transformation of the data, which is then separated with a linear hyperplane. SVM data must be scaled as the algorithms are sensitive to the magnitude range of the data [33].

K-nearest neighbours (KNN) is a clustering algorithm which classifies data based on the closest neighbours of the training set. A K predefined number of neighbours is selected. Each new feature is compared to the same feature from the training data, and the closest K labels are recorded. The label

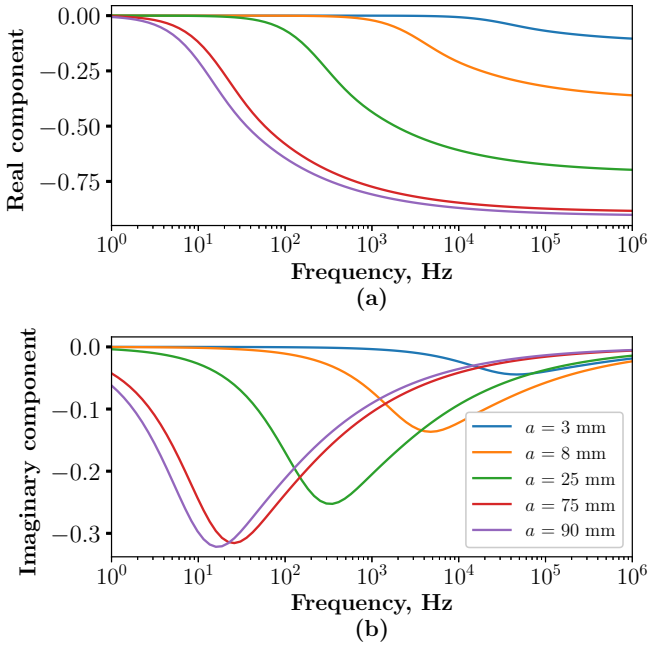

Fig. 2. The real (a) and imaginary (b) components of different sized spheres that have a conductivity of 16.24 MS/s (28% ICAS) and are measured 3mm away from the surface.

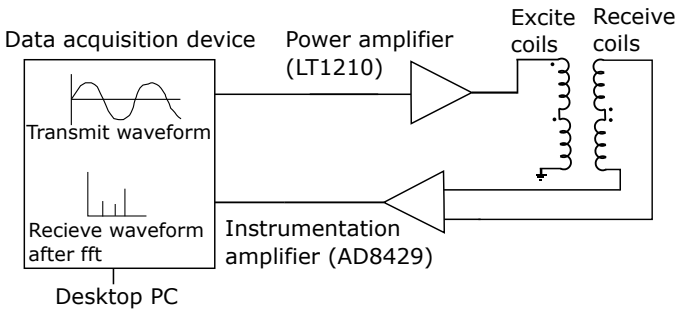

Fig. 3. Schematic of analogue electronics for the MetalID system.

with the largest number of nearest neighbours from a particular class is assigned to that data point.

Ensemble classifiers use a combination of multiple decision trees. Random forest (RF) and Extra randomised trees (ET) algorithms contain decision trees, whose individual results are combined and used to determine the label. The decision is determined by the majority or the average of the predictions of all trees. Adaboost is similar to RF and ET; but instead uses multiple small decision trees. Once a base tree is created, it is tested on the training data, the weight of misclassified training data is increased for the next predictor [34]. The result is decided by a majority vote.

III. Method

A. MetalID system

The MetalID sensor was first described in O'Toole et al. [9] with the solenoid design reported in [28]. A schematic of the system is shown in Fig. 3. The system comprises:

1) A sensing element or solenoid array.
2) Front-end analogue drive and receive electronics.
3) A Red Pitaya STEM 125-14 for data acquisition.

The sensing element consists of an inner excite coil with 32 turns wrapped around a 10 mm diameter acetyl former containing two 6 mm diameter ferrite rods (Fair-Rite 4077276011). The excite coil generates the excitation magnetic field H_{ex}, to induce eddy currents in the test object.

This structure is enclosed by a pair of outer receive coils, with 600 turns each wrapped around a 16 mm acetyl former and wound in opposition to form a gradiometer that cancels the effect of the excitation. This receive coil is used to measure the secondary magnetic field H_{rx} induced by the test object. We denote the complex frequency component of the voltage emf induced in the receive coil by the field H_{rx} as $V_{rx}(f)$.

The complete sensing element is screened by an aluminium cylinder with one end left open to form the sensing interface with the test pieces. The front-end analogue electronics consists of a LT1210 (Linear Technology), power amplifier which drives the excite coil with an oscillating current, and a AD8429 low-noise instrumentation amplifier (Analog Devices) which provides 40 dB gain on the measured emf.

The Red Pitaya data acquisition system synchronously outputs a transmit waveform to the power amplifier to drive the excitation coil, and measures the receive coil voltage output from the low noise amplifier. The transmit waveform is generated by a 12-bit DAC sampling at 12.5 MSPS. The receive waveform is measured using a 14-bit ADC sampling at 125 MSPS. The result is processed on an FPGA. The signal is first downsampled by a factor of 50 using an FIR filter and decimation process, then input to an FFT with a 4096-element buffer to obtain individual frequency components.

The MetalID sensor was used to obtain MIS measurements at frequencies from 3 KHz to 90 KHz in intervals of 3 KHz. The results are referenced to a calibration target, a 10 x 20 mm ferrite cylinder (material 4B1, Ferroxcube), in-line with previous research [9] [28]. The process for a frequency sweep of a single test sample was as follows:

1) 15 background frequency sweeps (scans) were taken and averaged where no test sample was present on the sensor. We denote the background scan $V_{rx,bkgnd}$.
2) The ferrite calibration target was placed on the sensor and scanned. This result is denoted $V_{rx,calib}$.
3) The test sample was placed on the sensor and scanned. This result is denoted $V_{rx,sample}$.

The ferrite piece is used as a reference as it has a constant permeability and negligible conductivity across the frequency range of interest. Therefore, it can be shown from (1) that the induction spectra H_{rx}/H_{ex} for the ferrite becomes purely real (zero imaginary) and uniform across the frequency range.

Denote the relative magnetic or mutual inductance, i.e. referenced to the ferrite, as $M(f) \propto H_{rx}/H_{ex}$. This result is obtained from the measurements described for a frequency f using the following:

$$M(f) = M' + jM'' = \frac{V_{rx,sample} - V_{rx,bkgnd}}{V_{rx,calib} - V_{rx,bkgnd}} \qquad (2)$$

where M' and M'' are the real and imaginary components respectively. The MIS sensor will be used independently and together with the results from an imaging system.

B. Imaging system

We propose that the visual characteristics of the scrap metal fragments (test samples) can complement induction measurements as features to classify the material. This work focuses on extracting colour, specifically the red, green and blue (RGB), and hue, saturation, and value (HSV) colour components for each test sample. Sample colour has the potential to distinguish between metals with high colour contrasts, for example, red metals (brass, copper, etc) from white metals (aluminium, etc).

Static images of each sample are taken with the induction measurements using a bespoke imaging rig, as shown in Fig. 4. The rig consists of a camera, image processing system and lighting dome. The MetalID sensor is located underneath the rig, housed in an acrylic box.

Images were taken using a Raspberry Pi 4 Model B 4 GB with a Raspberry Pi High-Quality Camera Module and a 3MP C-Mount 8 to 50 mm Zoom Lens. The lens captures images at 1920x1088 quality. The Raspberry Pi was programmed in Python 3.7, with the OpenCV2 V4.1.2 [35] and PiCamera V1.3 libraries to control the camera and process images.

The quality of light is a critical component for any vision system; it allows easier feature extraction and higher quality

images. A diffused light source is used to provide consistent illumination for each test sample. This was achieved using a 3D printed grey lighting dome and LED strips. The design of the lighting dome allows the camera to be mounted above the induction sensor at a sufficient distance to prevent interference.

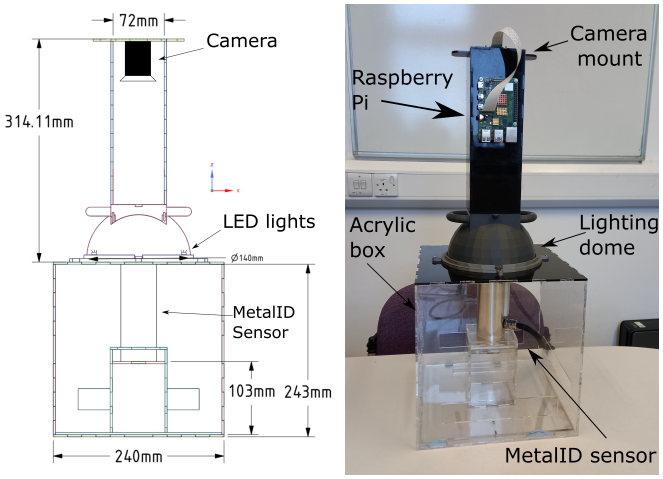

Fig. 4. Mechanical drawing and the built version of the imaging and induction system.

The camera images are processed to remove the background and extract a single colour, representative of the whole test sample in both RGB and HSV colour spaces. Background removal is performed by taking a series of images over 15 seconds while the camera rig is empty. These images are used to parameterise a 'Mean of Gaussian' background subtractor in OpenCV. The base of the lighting dome is kept black to facilitate this. Once this process is complete, a scan is run by placing the test piece onto the centre of box directly below the camera. The lighting dome is then secured, and an image and induction measurement are taken sequentially.

To extract a colour feature-set for the test sample, the image with background removed is first reduced to 50x50 pixels to increase the computational speed. A 2-means clustering algorithm is then applied to separate the pixels into two groups. One cluster group is the residual black background pixels and is ignored. The second group constitute foreground pixels of the sample. A mean average is taken of the foreground pixels across each colour component (RGB) to obtain a single RGB set representative of the sample. For HSV, the RGB image is converted to HSV first and the discussed process followed.

C. Test samples

Six datasets were used, which consisted of mixed non-ferrous metal and stainless steel from different waste streams sourced from commercial material recovery facilities. The waste streams include 'Zorba' (3 to 8 mm) and 'Zurik' (8 to 25 mm) [36], biomass incinerator metals (BIM), fridge metals, and window frames (WF) in two different size ranges (8 to 25 mm and 25 to 75 mm). Zorba consists of shredded non-ferrous metals and is predominantly aluminium, whereas Zurik is predominantly stainless steel [36]. BIM consists of metals that have been through an incinerator, leading to surface

TABLE II
THE METALS PRESENT WITHIN THE DIFFERENT DATASETS.

	Waste streams (datasets)					
	BIM	Window Frame	Zorba	Fridge metals	Zurik	Window Frame
Size (mm)	8 to 25	8 to 25	3 to 8	25 to 75	8 to 25	25 to 75
Aluminium	1	55*	30*	60*	0	13*
Titanium alloy	0	0	1	0	0	0
Stainless steel	2	0	0	2	33*	14*
Zinc	1	33*	6	4	2	7
Nickel	0	0	0	0	2	0
Iron	0	0	0	0	2	0
Copper	6	0	15	4	1	0
Brass	73*	3	30*	1	2	2
Bronzes	8	0	5	19	3	0
Nickel alloy	1	0	0	1	0	0
Nickel silver	0	1	1	0	1	0
Total	92	92	88	91	46	36

*Metal pieces that comprise more than 20% of the dataset.

contamination on all pieces. The fridge metal and window frame streams consist of shredded refrigerator and window frames. The differentiation of the input waste streams and size filtering are consistent with industry standards and are a realistic presentation for a material separator.

The metal samples in the datasets were measured with an XRF handheld device (Hitachi X-MET8000 Optimum). The analyser provided a metal composition and an industrial grade. The grade was used to label the pieces according to 11 output classes defined by material, such as copper, brass and stainless steel. These output classes are consistent with expected returns for a commercial materials separation process. The XRF analyser was not able to assign all metal pieces an industrial grade. In those cases, the pieces were labelled with an output class determined by the dominant element in the metal composition, e.g. samples with over 90% zinc were labelled as 'Zinc'. Samples where the class was unclear from the composition were removed from the dataset.

The input waste streams, output classes, and the number of samples for each are shown in Table II. For the results that follow, we will not derive a classifier for any class label within a dataset where the number of samples is less than 20% of the total number of samples within that dataset; this is to ensure that enough pieces are present for training and testing. For example, we do not determine a classifier for aluminium in the BIM dataset as there is only one piece available. On the other hand, we can determine a classifier for brass as this makes up a significant proportion of the BIM dataset (Brass $\sim$65% / Not Brass $\sim$35%). If more than one metal class is $>$20%, such as aluminium and brass in 3 to 8 mm Zorba, we design two separate binary classifiers (one for each metal) using all samples in the dataset. In practice, industrial separators can only sort by binary classification (Class / Not Class). To remove multiple materials, one metal would be removed from the waste stream first, then the next metal by re-testing the filtered material.

D. Machine learning

The python library Scikit-learn V0.22.2 [34] was used for the training and implementation of the machine learning models. The models had different inputs depending on whether the

colour was used as a feature. When the model used induction only, there was a total of 60 inputs which consisted of the real and imaginary components of each frequency measured. When the colour components were used, there was a total of 66 inputs, which consists of the 60 induction measurements, R, G, B, H, S and V.

All features are scaled between 0 and 1 prior to use; this is essential for SVM and KNN algorithms [33]. It is important to constrain a machine learning model's hyperparameters to reduce overfitting. The models were constrained by selecting a predefined range for the hyperparameters. The GridSearchCV function was used find the combination of hyperparameters that achieved the highest accuracy.

SVM [37] has two hyperparameters: the first was the regularisation, set to a range of 50 values between 0.01 and 100 increasing logarithmically. The second was the kernel, which refers to either linear, polynomial or RBF. All three kernels were evaluated. KNN has one hyperparameter: the number of neighbours. The number of neighbours ranged from 1 to half the number of samples within the dataset.

RF and ET have two hyperparameters: the number of estimators, which refers to the number of decision trees used, and the maximum number of features to consider when looking for the best split. The number of estimators and the maximum number of features ranged from 1 to 20. Adaboost has only one hyperparameter: the number of estimators which ranges from 10 to 200 in step intervals of 10.

The algorithms used in this study are considered more traditional machine learning algorithms. A disadvantage of the traditional algorithms is that they are known to have high variance [38]. In addition, small datasets lead machine learning algorithms to overfit the training data [39]. Future training of models would benefit from a larger dataset consisting of more metal samples to reduce the risk of overfitting by the model. Different techniques, such as dropout, can be applied to algorithms such as deep artificial neural networks (ANNs) to reduce overfitting, which would help with small datasets [39]. Future design and research may benefit from the use of more complex algorithms such as ANNs.

E. Analysis and comparison

The F1 score is used to compare performance between algorithms and feature sets. The F1 score is the harmonic mean of the precision and recall [33]; this means that the F1 score will only be high if both precision and recall are high [33]. The precision and the recall are also calculated. In what follows, we will refer to precision as purity-rate and recall as recovery-rate. in line with the terminology more familiar to the material recovery industry. Purity-rate describes the proportion of correct material within the sorted product after separation. Recovery-rate describes the proportion of material correctly recovered from the total available within the input waste stream. These terms are formally defined as follows, noting the interchangeability with precision and recall:

$$\mathbf{Purity} = \frac{\mathbf{TP}}{\mathbf{TP} + \mathbf{FP}}, \quad \mathbf{Recovery} = \frac{\mathbf{TP}}{\mathbf{TP} + \mathbf{FN}}$$

TABLE III
RECOVERY AND PURITY RATES FOR HIGHEST F1 SCORED ALGORITHMS THAT USE MAGNETIC INDUCTION ONLY.

Desired metal	Dataset	Algorithm	F1 score	Recovery rate (%)	Purity rate (%)
Stainless steel	8 to 25 mm Zurik	RF	0.9605	99.09	93.25
	25 to 75 mm WF	RF, ET	1	100	100
Brass	3 to 8 mm Zorba	ET	0.5387	54.67	53.82
	BIM	SVM	0.898	97.53	83.34
Zinc	8 to 25 mm WF	SVM	0.7924	81.50	77.28
Aluminium	3 to 8 mm Zorba	SVM	0.6024	70.33	52.73
	Fridge metals	SVM	0.8762	93.17	82.76
	8 to 25 mm WF	SVM	0.9003	89.45	90.64
	25 to 75 mm WF	SVM	0.8802	96.15	81.26

$$\mathbf{F_1} = \mathbf{2x}\frac{\mathbf{purity} \times \mathbf{recovery}}{\mathbf{purity} + \mathbf{recovery}} = \frac{\mathbf{TP}}{\mathbf{TP} + \frac{\mathbf{FN}+\mathbf{FP}}{\mathbf{2}}}$$

where $\mathbf{TP}, \mathbf{TN}, \mathbf{FP}, \mathbf{FN}$ are true positives, true negatives, false positives and false negatives, respectively. Stratified K-fold cross-validation is used to evaluate the machine learning models. K-fold cross-validation splits the input dataset into 'K' predefined groups or folds, then trains with all the data except for one-fold which is reserved for testing. This process repeats until all folds have been evaluated as a test-set. Stratified K-fold cross-validation also preserves the ratio of each class within the folds. We choose $K = 10$ for the work that follows.

The relatively small size of each dataset means that performance can be sensitive to the order of the samples. Therefore, the process explained in this section was repeated 10 times with the datasets shuffled at each iteration to randomise the order. Each algorithm was trained and tested with the same combination of shuffled data to allow a fair comparison. The mean average F1 score, purity and recovery rate from across the 10 shuffles are used to present the results within this paper.

IV. RESULT AND DISCUSSION

In the first part of this section, we explore the efficacy of using the magnetic induction spectra alone as a feature set, using the apparatus and method described in section 3.A. In the second part, we explore the improvement from combining the magnetic induction spectra with sample colour to create a wider feature set, with colour measured using the imaging system described in section 3.B.

Fig. 5 shows the F1 scores when classifying stainless steel, brass, zinc and aluminium across the six datasets described in section 3.C. The results are obtained using five machine learning models reported in section 2.B. The models include the SVM and KNN algorithms, and the three ensemble classifiers: Random Forests (RF), Extra Randomised Trees (ET), and Adaboost. Table. III summarises the highest performing models according to the F1 score across each dataset, with their associated purity and recovery rates, for the four different output classes (metal types) using the magnetic induction spectra as the sole feature set.

From Table. III, stainless-steel was classified with a $>$99% recovery and $>$93% purity rate; this was achieved using random forest and extra randomised trees.

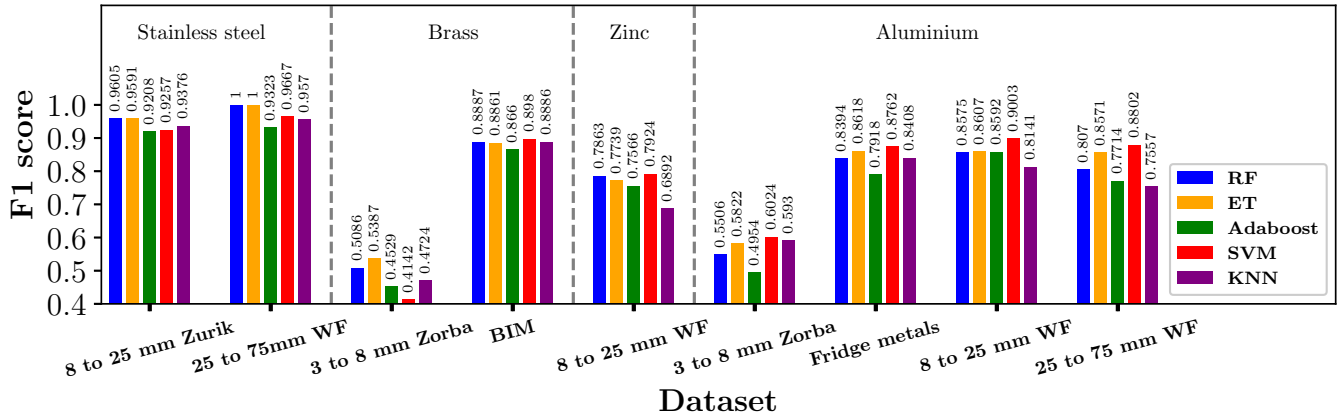

Fig. 5. Classification results of magnetic induction feature only of different machine learning algorithms.

TABLE IV
RECOVERY AND PURITY RATES FOR HIGHEST F1 SCORED ALGORITHMS THAT USE MAGNETIC INDUCTION ONLY.

Dataset method	F1	Recovery	Purity
Oversampling	0.9488	93.23	96.63
Undersampling	0.8714	91.76	83.10
Oversampling and undersampling	0.9195	88.61	95.66

Brass within the BIM dataset obtained 97.53% recovery and 83.34% purity rate using SVM. It is clear from Fig. 5 that this performance was consistent across all classifiers (F1 score from 0.866 to 0.898). The total number of brass samples was 73 compared to the 19 non-brass samples; this imbalance weighted towards brass could lead to better results. To test the brass results within BIM, oversampling, undersampling, and a combination of both were applied to the dataset, and the same machine learning process was taken. Oversampling involves copying the samples in the minority class, and undersampling involves removing samples from the majority class. The BIM dataset was reproduced using the following rules ten times each, which produced 30 new datasets:

1) Oversampling: copy a random number, between 15 and 19, of non-brass pieces
2) Undersampling: remove a random number, between 18 and 25, of brass pieces
3) Oversampling and under sampling: apply both 1 and 2 to the dataset

The results obtained with the new BIM datasets are shown in Table. IV. Only the undersampling case showed a reduced F1 score compared to table III, and only by a difference of 0.02. This indicates that even with the class imbalance, the results reported are what is expected.

This result for brass was not repeated with the 3 to 8 mm Zorba dataset, where classification fell to 54.67% recovery and 53.82% purity rate. Zinc achieved 81.5% recovery and 77.28% purity rate using random forest. The result was relatively consistent across the machine learning models except for KNN, which had an F1-score $\sim$0.1 lower than the median.

Aluminium achieved F1 scores between 0.87 to 0.90 across three datasets, with recovery and purity rates between 89.45 to 96.15% and 81.26 to 90.64%, respectively. However, the 3 to 8 mm Zorba dataset obtained a lower recovery and purity rate of 70.33% and 52.73%. The results for aluminium with the 3 to 8 mm Zorba were consistent with the brass classification

TABLE V
RECOVERY AND PURITY RATES FOR HIGHEST F1 SCORED ALGORITHMS THAT USED MAGNETIC INDUCTION AND COLOUR FEATURES.

Desired metal	Dataset	Algorithm	F1 score	Recovery rate (%)	Purity rate (%)
Stainless steel	8 to 25 mm Zurik	RF	0.9692	100	94.04
	25 to 75 mm WF	RF, ET	1	100	100
Brass	3 to 8 mm Zorba	SVM	0.8501	89.09	87.2
	BIM	SVM	0.8956	98.63	82.05
Zinc	8 to 25 mm WF	ET	0.8968	94.5	85.38
Aluminium	3 to 8 mm Zorba	SVM	0.8221	91.00	75.00
	Fridge metals	ET	0.9704	95.09	99.07
	8 to 25 mm WF	RF	0.9899	98.16	99.83
	25 to 75 mm WF	SVM	0.8489	88.47	81.69

results, which also showed a marked performance drop across the same dataset. This reduction is due to the presence of aluminium alloys in the Zorba with similar conductivities to brass. From (1), the induction spectra is a function of the sample conductivity and morphology. When the induction spectra is used as a feature-set, the machine learning models effectively classify the material according to conductivity, while minimising sensitivity to sample size and shape.

Aluminium as an element has a conductivity of 65% ICAS [40]. However, within the 3 to 8 mm Zorba dataset, most aluminium pieces present are cast AL-383 and AL-384, with conductivities around 23% ICAS [40]. Cast aluminium conductivity is similar to brass, with around 26% ICAS [41]. By contrast, other datasets are mostly wrought aluminium alloys (AA-1100, AA-4343, AA-6070, AA-6151) with 42 to 59% ICAS [41]. For example, Zinc with 28% ICAS [42], is well separated in the the window frame (WF) dataset because it is mostly compared to wrought aluminum. The variation in conductivity poses a limitation on this approach when attempting to classify distinct elements with similar conductivities. This limitation should be acknowledged during training a model as it would be better to group metals of similar conductivity together, such as cast aluminium and brass when only magnetic induction is used. However, it also presents an opportunity to separate alloys with high conductivity contrasts, for example, wrought from cast aluminium.

In Table III, we found poor performance within the Zorba dataset between brass and aluminium with similar conductivity. We hypothesise adding sample colour to the magnetic induction spectra as a combined feature set will improve this result. Fig. 6 shows each machine learning model's F1 score

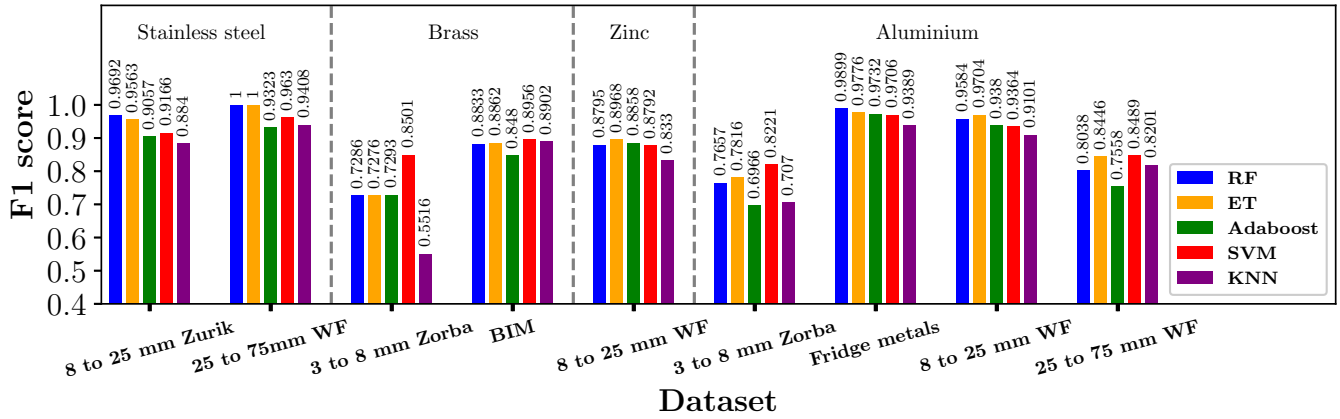

Fig. 6. Classification results of magnetic induction and colour features of different machine learning algorithms.

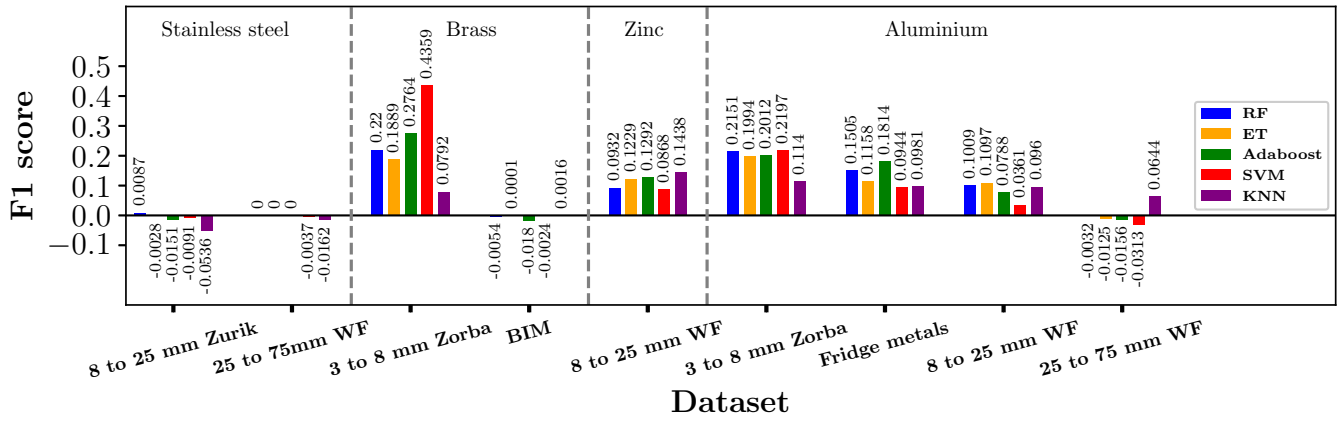

Fig. 7. The change in F1 score when colour is used as a feature with magnetic induction.

when RGB and HSV parameters are included as features. RGB and HSV are extracted using the method outlined in section 3.B. Fig. 7 shows the difference between Fig. 6 and the previous magnetic induction spectra results presented in Fig. 5. Table V summarises the recovery and purity rates of the highest performing results for each metal class.

Stainless steel, which already had a high F1 score across the Zurik and window frame datasets, does not improve with colour; this shows that MIS alone is sufficient to classify stainless steel. Similarly, colour did not significantly improve the classification accuracy for brass within BIM dataset; this is unsurprising given the extent of surface contamination on the BIM metal pieces caused by incineration, which leaves all the pieces with a similar colour. On the other hand, zinc showed a notable improvement in classification when using colour. The recovery increased by 13 and purity by 8.1 percentage points. The most significant improvement was for brass and aluminium within the 3 to 8 mm Zorba dataset. For brass, the improvement was most evident for the SVM model, where F1 score increased from 0.4142 to 0.8501, yielding a recovery and purity rate of 89.09% and 87.2% respectively. Aluminium F1 scores increased with colour across all datasets apart from the 25 to 75 mm window frame. In the 3 to 8 mm Zorba dataset, recovery and purity rate improved to 91% and 75%. These results support our previous hypothesis that colour contrast can improve the classification of metals when conductivities are similar and no significant surface contamination is present.

A problem which was not addressed in this study is that on an industrial conveyor the pieces may overlap, but this is a potential challenge in all dry classification methods. However, we expect that the use of a vibrator feeder would reduce the chance of metals overlapping.

Rigorous performance measurements of calculation speed for the machine learning models is beyond the scope of the present work. However, our preliminary estimates indicate classification times of less than 1 ms for all algorithms, apart from Adaboost which was slightly longer classifying in $<$3 ms. A classification speed of $<$1 ms is practical for an industrial separator. For example, typical conveyor speed of $\sim$2 m/s, and distances of up to 0.5 m between the sensing element and ejector manifold would yield 250 ms of available classification time.

V. Conclusion

Magnetic induction spectroscopy offers a new approach for the classification of non-ferrous scrap metals in the recycling and waste recovery sector. The authors first posited an MIS approach using two-frequency component classification [28]. However, the effectiveness was found to be limited on classes of waste pulled from commercial production lines [9].

This paper presents the first results on using multi-frequency magnetic induction spectroscopy. This progression from O'Toole et al. [9] uses more frequencies across a wider spectrum to derive features for classification; trading the simplicity of a two-frequency-component approach for the information provided by a fuller induction spectra. We

demonstrate the use of multi-frequency MIS to successfully classify valuable non-ferrous scrap metals, including stainless steel, brass, aluminium, and zinc, from within different industry-standard waste streams (datasets), such as Zorba and Zurik. Magnetic induction spectroscopy could achieve a >99% recovery rate and >93.25% purity rate when classifying stainless steel. Good classification performance was found generally across the different metals and datasets, with recovery and purity rates greater than 80% in most cases. MIS achieved 98.63% recovery and 82.05% purity of brass from the biomass incinerator metals (BIM) dataset, indicating immunity to surface contamination in contrast to optical or some x-ray techniques. The exception in performance was the 3 to 8 mm Zorba dataset, where aluminium and brass classification fell to between 50% and 70% purity and recovery rates. This is attributed to the aluminium AL-384 alloy present in the dataset, which has a conductivity of 23% ICAS, close to the conductivity of brass and provoking misclassification.

Introducing colour components (RGB, HSV) as additional features combined with MIS improved classification performance for brass, zinc and aluminium metals across the majority of datasets. This improvement was the most marked across the previously poorly performing 3 to 8 mm Zorba, where the recovery and purity rates improved to a more acceptable 91% and 75% respectively for aluminium, and 89.09% and 87.2% for brass. Across the different machine learning models used, random forest, extra randomised trees, and SVM yielded better results than other algorithms.

Magnetic induction spectroscopy independently or combined with colour parameters is shown to be an effective and robust method for the classification and recovery of non-ferrous scrap metals. MIS alone is insensitive to surface contamination on the sample, although limited where conductivity contrasts between metals are poor. The support of colour components substantially improves performance in this case at the cost of being subject to surface contamination. There is some balance to be achieved in weighting MIS measurements against colour between classification capability and sensitivity to surface contamination, dependent on the characteristics of the waste stream being sorted. Nevertheless, our findings suggest that for general zorba as tested here, the combination of the two approaches will supersede either method individually.

The effectiveness of colour is subject to good lighting conditions, which was achieved in this study with the lighting dome. However, industrial conditions would certainly present a more variable and challenging environment to deliver this consistent illumination, noted by Kutila et al. [22]. There is scope for the use of enclosures or hoods over the conveyor to control light sources, such as the scheme in Tachwali et al. [43], using diffused and polarised light sources such as in Pramerdorfer and Kampel [44], or elliptical reflectors in Barnabé et al. [45]. This could further be complemented with air to blow away any dust particles – a standard approach in industry. An MIS and colour system would need to be partnered with a mechanical mechanism to eject the classified scrap metal into the required bins. Ejection could be achieved with air jets, which is industry standard [4], [10]. A limitation of the magnetic induction and colour sensors is the inability to separate non-ferrous metals which have similar conductivity and surface contamination. Additional limitations of this method are that induction measurements ideally require a metal piece close to the sensor, which can be difficult with a bouncing conveyor and rolling pieces. The feasibility of this technology has been demonstrated herein, and we continue to develop a mixed-metal separation solution for high-throughput and mid-cost recovery of some of the most common and valuable non-ferrous materials.

ACKNOWLEDGMENT

The authors would like to thank the UK Engineering and Physical Sciences Research Council (Grant ref EP/W021013/1) and the Innovate UK (contract ref 72207) for their financial support and Magnapower Equipment Ltd for their advice and technical support.

REFERENCES

[1] J. A. S. Green, "Aluminium Recycling and Processing for Energy Conservation and Sustainability," p. 271, 2007.
[2] P.-A. Enkvist and P. Klevnäs, "The Circular Economy- A powerful force for climate mitigation," p. 176, 2018.
[3] G. Gaustad, E. Olivetti, and R. Kirchain, "Improving aluminium recycling: A survey of sorting and impurity removal technologies," Resources, Conservation and Recycling, vol. 58, pp. 79–87, 2012.
[4] D. Raabe, C. C. Tasan, and E. A. Olivetti, "Strategies for improving the sustainability of structural metals," Nature, vol. 575, pp. 64–74, 2019.
[5] A. Minter, "Where America Recycles, 2008.
[6] L. Brooks and G. Gaustad, "The Potential for XRF & LIBS Handheld Analyzers to Perform Material Characterization in Scrap Yards," Journal of Sustainable Metallurgy, vol. 7, no. 2, pp. 732–754, 2021.
[7] L. Brooks and G. Gaustad, "Positive material identification (pmi) capabilities in the metals secondary industry: an analysis of xrf and libs handheld analyzers," Minerals, Metals and Materials Series, 2019.
[8] M. Cho, S. Park, E. Kwon, S. Jeong, and K. Park, "A waste metal sorting system using LIBS classification," IEEE International Symposium on Industrial Electronics on Industrial Electronics, pp. 451–454, 2019.
[9] M. D. O'Toole and A. J. Peyton, "Classification of Non-ferrous Scrap Metal using Two Component Magnetic Induction Spectroscopy," 2019 IEEE Sensors Applications Symposium (SAS), 2019.
[10] S. P. Gundupalli, S. Hait, and A. Thakur, "A review on automated sorting of source-separated municipal solid waste for recycling", Waste Management, 2017.
[11] L. Brooks, G. Gaustad, A. Gesing, T. Mortvedt, and F. Freire, "Ferrous and non-ferrous recycling: Challenges and potential technology solutions," Waste Management, vol. 85, pp. 519–528, 2019.
[12] M. B. Mesina, T. P. De Jong, and W. L. Dalmijn, "New developments on sensors for quality control and automatic sorting of non-ferrous metals," IFAC Proceedings Volumes, vol. 37, pp. 293–298, 2004.
[13] S. Kelly and D. Apelian, "Automotive aluminium recycling at end of life: a grave-to-gate analysis," Worcester Polytechnic Institute, 2016.
[14] N. Dholu, J. R. Nagel, D. Cohrs, and R. K. Rajamani, "Eddy current separation of nonferrous metals using a variable-frequency electromagnet," KONA Powder and Particle Journal, no. 34, pp. 241–247, 2017.
[15] Y. R. Smith, J. R. Nagel, and R. K. Rajamani, "Eddy current separation for recovery of non-ferrous metallic particles: A comprehensive review," Minerals Engineering, vol. 133, no pp. 149–159, 2019.
[16] J. R. Nagel, D. Cohrs, J. Salgado, and R. K. Rajamani, "Electrodynamic Sorting of Industrial Scrap Metal," KONA Powder and Particle Journal, vol. 37, pp. 258–264, 2020.
[17] Y. Li, X. Qin, Z. Zhang, and H. Dong, "A robust identification method for nonferrous metal scraps based on deep learning and superpixel optimization," Waste Management and Research, vol. 39, no. 4, pp. 573–583, 2021.
[18] A. Picón, O. Ghita, A. Bereciartua, et al., "Real-time hyperspectral processing for automatic nonferrous material sorting," Journal of Electronic Imaging, vol. 21, no. 1, 2012.

[19] A. Picón, O. Ghita, P. F. Whelan, and P. M. Iriondo, "Fuzzy spectral and spatial feature integration for classification of nonferrous materials in hyperspectral data," IEEE Transactions on Industrial Informatics, vol. 5, no. 4, pp. 483–494, 2009.

[20] G. Candiani, N. Picone, L. Pompilio, M. Pepe, and M. Colledani, "Characterization of fine metal particles derived from shredded WEEE using a hyperspectral image system: Preliminary results," Sensors, vol. 17, no. 5, 2017.

[21] M. B. Mesina, T. P. R. De Jong, and W. L. Dalmijn, "Improvements in separation of non-ferrous scrap metals using an electromagnetic sensor," Physical Separation in Science and Engineering, vol. 12, no. 2, 2003.

[22] M. Kutila, J. Viitanen, and A. Vattulainen, "Scrap metal sorting with colour vision and inductive sensor array," International Conference on Computational Intelligence for Modelling, Control and Automation, and International Conference on Intelligent Agents, Web Technologies and Internet Commerce, vol. 2, pp. 725–729, 2005.

[23] M. Lu et al., "Determination of Surface Crack Orientation Based on Thin-Skin Regime Using Triple-Coil Drive–Pickup Eddy-Current Sensor," IEEE Transactions on Instrumentation and Measurement, vol. 70, pp. 1-9, 2021.

[24] M. Lu, X. Meng, R. Huang, L. Chen, A. Peyton and W. Yin, "Measuring Lift-Off Distance and Electromagnetic Property of Metal Using Dual-Frequency Linearity Feature," IEEE Transactions on Instrumentation and Measurement, vol. 70, pp. 1-9, 2021.

[25] M. Lu, L. Chen, X. Meng, R. Huang, A. Peyton and W. Yin, "Thickness Measurement of Metallic Film Based on a High-Frequency Feature of Triple-Coil Electromagnetic Eddy Current Sensor," IEEE Transactions on Instrumentation and Measurement, vol. 70, pp. 1-8, 2021.

[26] B. Dekdouk, C. Ktistis, L. A. Marsh, D. W. Armitage, and A. J. Peyton, "Towards metal detection and identification for humanitarian demining using magnetic polarizability tensor spectroscopy," Meas. Sci. Technol., vol. 26, no. 11, 2015.

[27] L. A. Marsh et al., "Combining Electromagnetic Spectroscopy and Ground-Penetrating Radar for the Detection of Anti-Personnel Landmines," Sensors, vol. 19, no. 15, 2019.

[28] M. D. O'Toole, N. Karimian, and A. J. Peyton, "Classification of nonferrous metals using magnetic induction spectroscopy," IEEE Transactions on Industrial Informatics, vol. 14, no. 8, pp. 3477–3485, 2018.

[29] K. C. Williams, M. D. O'toole, L. A. Marsh, and A. J. Peyton, "Classification of batteries in waste streams using magnetic induction spectroscopy," 2022 Sensors Applications Symposium (SAS), pp. 1-6, 2022

[30] J. R. Wait, "A conducting permeable sphere in the presence of a coil carrying an oscillating current," Canadian Journal of Physics, vol. 31, no. 4, pp. 670–678, 1953.

[31] M. L. Honke and C. P. Bidinosti, "The metallic sphere in a uniform ac magnetic field: A simple and precise experiment for exploring eddy currents and non-destructive testing," American Journal of Physics, vol. 86, no. 6, pp. 430–438, 2018.

[32] R. Ludwig and P. Bretchko, RF Circuit Design, Theory and Applications, 2nd. Pearson, p. 704, 2009.

[33] A. Ǵeron, "Hands-On Machine Learning with ScikitLearn, Keras, and TensorFlow - Concepts, Tools,and Techniques to Build Intelligent Systems", 2nd Edition, 2019.

[34] F. Pedregosa, R. Weiss, M. Brucher, et al., "Scikit-learn: Machine Learning in Python," Journal of Machine Learning Research, vol. 12, no. 85, pp. 2825–2830, 2011.

[35] G. Bradski, "The OpenCV Library," Dr. Dobb's Journal of Software Tools, 2000.

[36] ISRI, "Scrap Specifications Circular," p. 60, 2021.

[37] C.-C. Chang and C.-J. Lin, "LIBSVM: A Library for Support Vector Machines," Association for Computing Machinery, vol. 2, p. 27, 2011.

[38] S. Shirmohammadi and H. Al Osman, "Machine Learning in Measurement Part 1: Error Contribution and Terminology Confusion," IEEE Instrumentation and Measurement Magazine, vol. 24, no. 2, pp. 84–92, 2021.

[39] H. Al Osman and S. Shirmohammadi, "Machine Learning in Measurement Part 2: Uncertainty Quantification," IEEE Instrumentation and Measurement Magazine, vol. 24, no. 3, pp. 23–27, 2021.

[40] J. R. Davis, "ASM Handbook aluminium and aluminium Alloy," p. 729, 1993.

[41] J. R. Davis, "Copper and Copper Alloys Edited," p. 869, 2001.

[42] F. Cardarelli, "Materials Handbook: A Concise Desktop Reference", 2nd Edition, p. 1340, 2008.

[43] Y. Tachwali, Y. Al-Assaf, and A. R. Al-Ali, "Automatic multistage classification system for plastic bottles recycling," Resources, Conservation and Recycling, vol. 52, no. 2, pp. 266–285, 2007.

[44] C. Pramerdorfer and M. Kampel, "PCB Recognition using Local Features for Recycling Purposes," VISAPP 2015 - 10th International Conference on Computer Vision Theory and Applications; VISIGRAPP, Proceedings, vol. 3, pp. 71–78, 2015.

[45] P. Barnabé, G. Dislaire, S. Leroy, and E. Pirard, "Design and calibration of a two-camera (VNIR and SWIR) hyperspectral acquisition system for the characterization of metallic alloys from the recycling industry," vol. 9534, pp. 167–178, 2015.

Kane C. Williams received the B.Eng (Hons.) degree in electronic engineering with industrial experience from The University of Manchester in 2020. He currently is undertaking a Ph.D. at The University of Manchester. His research focuses on classifying and sorting scrap waste using machine learning and different sensors for non-destructive inspection. His research interests include machine learning, embedded systems and computer vision and sensor fusion.

Michael D. O'Toole received the M.Eng. (Hons.) degree in integrated engineering from the University of Reading in 2006, and the Ph.D. from the Wolfson School of Mechanical and Manufacturing Engineering, Loughborough University, in 2011. He was a Research Associate at The University of Manchester from 2011 to 2016 working primarily on magnetic induction systems for non-destructive inspection and characterisation. He was awarded a Leverhulme Trust Early Career Research Fellowship in 2016, and appointed lecturer in 2020. He is author and co-author of over 20 scientific publications and has recently filed his first patent. His research interests include signal processing, and sensor and instrumentation design, with a particular emphasis on magnetic induction systems for non-destructive testing.

Anthony J. Peyton received the B.Sc. degree in electrical engineering and electronics and Ph.D. in medical instrumentation from UMIST in 1983 and 1986, respectively. He was appointed Principal Engineer at Kratos Analytical Ltd. in 1989, developing precision electronic instrumentation for magnetic sector and quadrupole mass spectrometers. He returned to UMIST as a Lecturer and worked with the Process Tomography Group. He moved to Lancaster University in 1996 as Senior Lecturer, was promoted to Reader in electronic instrumentation in 2001 and Professor in 2004. Since 2004, he has been a Professor of Electromagnetic Tomography Engineering at the University of Manchester. He has been a Principal Investigator of numerous national and industry funded projects and a partner of ten previous EU projects. He is a co-author on over 110 international journal papers, two books, several hundred conference papers, and 12 patents in areas related to electromagnetics and tomography.